Monthly Notices
of the
ROYAL ASTRONOMICAL SOCIETY

MNRAS **486,** 2129–2136 (2019)
Advance Access publication 2019 March 27

doi:10.1093/mnras/stz875

Spectroscopic confirmation of the binary nature of the hybrid pulsator KIC 5709664 found with the frequency modulation method

A. Derekas,[1,2,3★] S. J. Murphy,[4,5] G. Dálya,[6] R. Szabó,[2,7] T. Borkovits,[2,8] A. Bókon,[9] H. Lehmann,[10] K. Kinemuchi,[11] J. Southworth,[12] S. Bloemen,[13] B. Csák,[1,2] H. Isaacson,[14] J. Kovács,[1,3] A. Shporer,[15] Gy. M. Szabó,[1,3] A. O. Thygesen[16] and Sz. Mészáros[1,3†]

Affiliations are listed at the end of the paper

Accepted 2019 March 21. Received 2019 March 21; in original form 2018 June 28

ABSTRACT

We started a program to search for companions around hybrid δ Sct/γ Dor stars with the frequency modulation method using *Kepler* data. Our best candidate was KIC 5709664, where we could identify Fourier peaks with sidelobes, suggesting binary orbital motion. We determined the orbital parameters with the phase modulation method and took spectroscopic measurements to confirm unambiguously the binary nature with radial velocities. The spectra show that the object is a double-lined spectroscopic binary, and we determined the orbital solutions from the radial velocity curve fit. The parameters from the phase modulation method and the radial velocity fits are in good agreement. We combined a radial velocity and phase modulation approach to determine the orbital parameters as accurately as possible. We determined that the pulsator is a hybrid δ Sct/γ Dor star in an eccentric binary system with an orbital period of ∼95 d and an eccentricity of 0.55. The measured mass ratio is 0.67. We analysed the pulsation content and extracted 38 frequencies with amplitudes greater than 20 μmag. At low frequencies, we found broad power excesses which are likely attributed to spots on the rotating surface of the lower mass component. We inferred rotation periods of 0.56 and 2.53 d for the primary and secondary, respectively.

Key words: binaries: spectroscopic – stars: individual: KIC5709664 – stars: oscillations.

1 INTRODUCTION

Due to very precise observations from the recent generation of space telescopes (such as CoRoT and *Kepler*), we know that almost all stars show some type of pulsation. It is also known that more than 50 per cent of stars are in binary or multiple systems (Alfonso-Garzón et al. 2014). Since binarity can influence the pulsation properties in different ways, it is very important to identify companions around pulsating stars if we aim for the determination of very accurate stellar properties.

Until recently, there were two photometric methods to discover companions of pulsating stars: observation of eclipses, or the O−C method in the case of monoperiodic pulsating stars. Of course, radial velocities (RVs) give unambiguous evidence for binarity. Shibahashi & Kurtz (2012) developed a method to find companions of multiperiodic pulsating stars in frequency space, which they called the frequency modulation (FM) method, and which makes the detection and study of these systems easier. In the case of a binary system in which at least one of the objects is a variable star with coherent oscillations, all of the relevant parameters of the system can be calculated using the frequency spectrum of the light curve: the orbital period, the semimajor axis and even the RVs and the mass function which are traditionally extracted from spectroscopic observations. The star and its companion orbit around the common centre of mass, hence the distance that the light from the star has to travel to the telescope is periodically shorter and longer than in the case where there is no companion. This phenomenon is called the light-time effect, and manifests itself as an FM in the Fourier spectrum of the light curve of the star, causing multiplets around every frequency peak.

Besides the FM method, Murphy & Shibahashi (2015) and Murphy, Shibahashi & Bedding (2016b) expanded and developed the phase modulation (PM) method (Murphy et al. 2014). Phase and frequency modulation are equivalent, and so the PM method can also be used for detecting binary systems using the stellar oscillations and calculating their orbital parameters. Because the PM method

★ E-mail: derekas@gothard.hu
† Premium Postdoctoral Fellow of the Hungarian Academy of Sciences

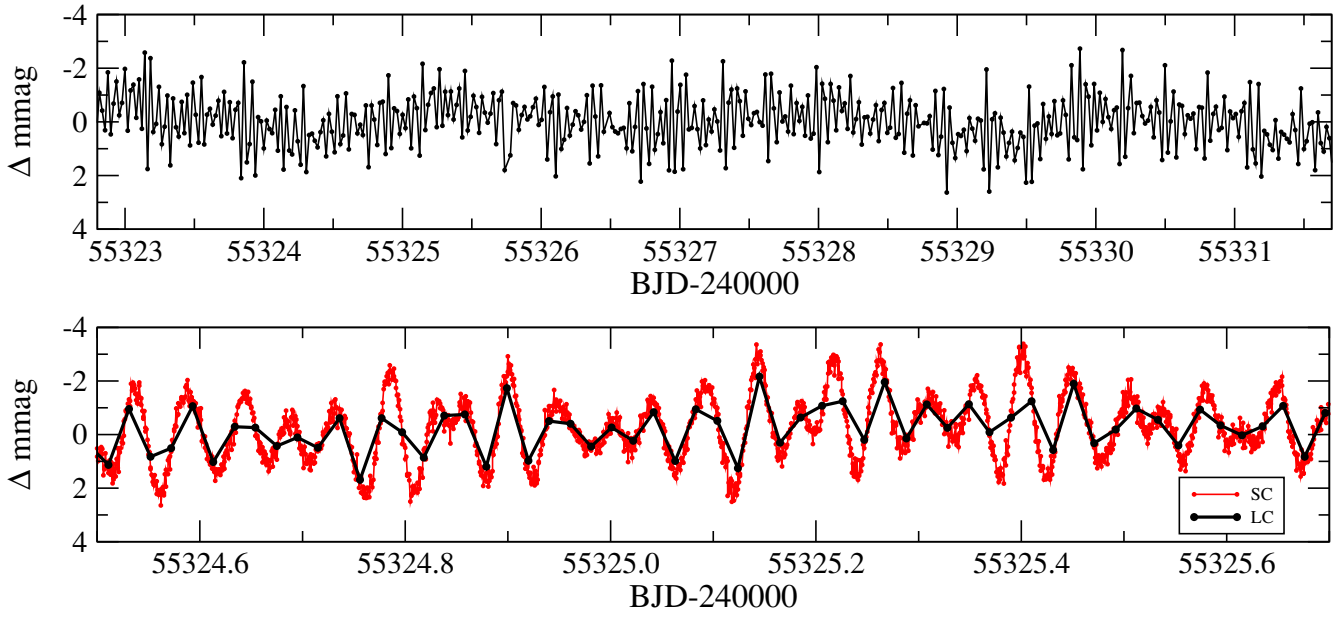

Figure 1. Top panel: a 9-d segment of the light curve. Bottom panel: 1-d segment of the light curve. The red symbols and line show the short cadence (60 s), the black symbols and line the long-cadence data (30 min).

involves binning of the light curve, it is sensitive only to systems where the period is greater than twice the length of bins.

Following the ground-breaking work of Shibahashi & Kurtz (2012), we started an investigation of hybrid δ Sct/γ Dor stars classified by Uytterhoeven et al. (2011) using long cadence data of the *Kepler* space telescope to find companions around them. These are A/F type main-sequence stars with coherent oscillations, lying in the instability strip of the Hertzsprung–Russell Diagram. They simultaneously show two types of non-radial pulsations: δ Sct low-order p modes with periods 0.008–0.42 d, and γ Dor low-degree high-order g modes with periods 0.3–3 d (Lampens et al. 2017; Sánchez Arias, Córsico & Althaus 2018). One of the biggest spectroscopic surveys of these hybrid pulsators was performed by Lampens et al. (2017), who investigated the binary fraction of 50 such hybrid pulsators based on RV measurements. They detected companions for 27 per cent of their sample. Murphy et al. (2018) investigated 2224 main-sequence A/F stars and found 341 non-eclipsing binaries with the PM method.

We studied 585 δ Sct, γ Dor, and hybrid δ Sct/γ Dor stars in our binary search project with the FM method. When it started in 2012, only *Kepler* Q0–Q10 data were available. One of the best candidates was KIC 5709664, which showed a consistent side-peak pattern at pulsation frequencies with the largest amplitudes. We then started to collect spectroscopic data to confirm its binarity.

The brightness of KIC 5709664 is Kp = 11.2 mag. Its basic physical parameters are $T_{\rm eff} = 6820$ K, $\log g = 4.4$ dex, [Fe/H] = −0.2 dex and vsin i= 71.4 km s^{-1} based on the spectra from the APOGEE Data Release 14 (Abolfathi et al. 2018). Murphy et al. (2018) identified it as a non-eclipsing binary using the PM method and determined the orbital parameters from the pulsation ($P_{\rm orb} = 95.03$ d; $a_1 \sin i = 50.5\,{\rm R}_\odot$; $e = 0.51$; $K = 23.1$ km s^{-1}) and listed it as a single-pulsator binary.

Here, we present the photometric and spectroscopic analysis of KIC 5709664. In Section 2, we describe the *Kepler* data used in the photometric analysis and the spectroscopic observations we took. In Section 3, we present our results of the photometric and spectroscopic orbit determination. The frequency analysis is discussed in Section 4 and finally we summarize our results in Section 5.

2 OBSERVATIONS

We used the *Kepler* data in the photometric analysis of KIC 5709664. A detailed description of the telescope and data processing can be found in Borucki et al. (2010), Gilliland et al. (2010), Jenkins et al. (2010a,b) and Koch et al. (2010). KIC 5709664 was observed in long-cadence mode (30-min exposures) for the full 4-yr mission (Quarters 0–17), while short-cadence observations (60-s exposures) were taken in Q2.2 and the whole of Q5. In this paper, we use all quarters (Q0–17) of the long-cadence observations, only. These constitute 65313 data points that have a time span of 1470.5 d and a duty cycle of 90.8 per cent.

We used the multiscale MAP light curve (Stumpe et al. 2014), obtained from KASOC.[1] A 9-d section of the light curve is plotted in Fig. 1.

We obtained medium- and high-resolution spectra at six observatories. The average S/N of these spectra was 40–80. The observations are described below and summarized in Table 1.

(i) We took one spectrum in 2012 May with the eShel spectrograph mounted on a 0.5-m Ritchey–Chrétien telescope at the Gothard Astrophysical Observatory (GAO), Szombathely, Hungary, in the spectral range 4200–8700 Å with a resolution of $R = 11\,000$.

(ii) We obtained three spectra in 2012 June with the 4.2-m William Herschel Telescope at La Palma using the ISIS spectrograph. It has dichroic filters which permit simultaneous observations in the blue and red arms. The blue arm used the H2400B grating and covered the 4170–4570 Å wavelength range at a resolution of 12 000. The red arm used the R1200R grating and covered 6040–6830 Å at a resolution of 8500.

[1] http://kasoc.phys.au.dk.

Table 1. Journal of observations.

Observatory	Wavelength range (Å)	Resolution	No. of spectra
WHT	4170–4570 and 6040–6830	12 000 and 8500	3
GAO	4200–8700	11 000	1
APOGEE	15 090–16 990	22 500	5
APO	3200–10 000	31 500	2
TLS	4540–7540	30 000	9
KECK	3640–7960	60 000	5

(iii) We obtained two spectra at Apache Point Observatory (APO), USA, using the ARCES Échelle spectrograph on the 3.5-m telescope with a resolution of $R = 31\,500$ in the spectral range 3200–10 000 Å. One spectrum was taken in 2012 October, and another in 2018 April.

(iv) We took nine spectra with the 2-m Alfred Jensch Telescope at Thüringer Landessternwarte Tautenburg in 2016 August and September. The spectrograph was used with a projected slit width of 2 arcsec providing a resolving power of $R = 30\,000$.

(v) We used spectra taken by the Apache Point Observatory Galactic Evolution Experiment (APOGEE; Majewski et al. 2017), part of the 3rd and 4th Sloan Digital Sky Survey (SDSS; Eisenstein et al. 2011; Blanton et al. 2017). APOGEE is a high-resolution ($R = 22\,500$) near-infrared survey, that is observing nearly 500 000 stars between 2011 and 2020 in the wavelength range of 15090–16990 Å (Wilson et al. 2012). We used five spectra from the 14th data release of SDSS (Abolfathi et al. 2018) which were taken in 2013 September and October.

(vi) We collected five spectra using the KECK I telescope equipped with the HIRES instrument with resolution of 60 000. The data were collected without the iodine cell. Spectra were taken between 2016 June and November and covered the 3640–7960 Å wavelength range. The technical information of the HIRES set-up is described in Shporer et al. (2016).

All spectra were reduced either using IRAF or a dedicated pipeline, then normalized to the continuum level. Except data from the APOGEE survey, the RVs were determined by cross-correlating the spectra with a well-matched synthetic template spectrum from the extensive spectral library of Munari et al. (2005). We used the 3850–6850 Å region in the cross-correlation, except for a 20 Å region around the Sodium D lines. Since the stellar rotation is fast, all the lines are broadened, so the spectra are dominated by the hydrogen lines. In Fig. 2, we show spectra focusing on the Hα line, illustrating the effect of the binary motion at different orbital phases.

All RVs were corrected to barycentric RVs. The APOGEE data are reduced by a dedicated pipeline, ASPCAP (García Pérez et al. 2016), which derives atmospheric parameters, rotation velocities, and chemical abundances by comparing observations with libraries of theoretical spectra. The measured RVs from all spectroscopic sources are listed in Table 2.

3 RESULTS

3.1 Photometric orbit determination

The binary orbit induces FM on the pulsation frequencies (Shibahashi & Kurtz 2012), generating sidelobes on each peak in the Fourier transform (Fig. 3). In order to obtain a set of excited, observed oscillation frequencies without sidelobes, we had to correct the observation times to the barycentre of the binary system. This first requires a photometric measurement of the orbital parameters, for which we used the PM method (Murphy et al. 2014; Murphy & Shibahashi 2015).

The Fourier transform of the *Kepler* light curve of KIC 5709664 is dominated by p modes near the long-cadence Nyquist frequency of 24.48 d^{-1} (Fig. 4). There is also variability at low frequencies, whose spectral window contributes noise at all frequencies and degrades the quality of a PM orbital solution. We therefore followed the methodology of Murphy, Bedding & Shibahashi (2016a) and high-pass filtered the light curve. It is important to note that we did this only for the PM analysis, and subsequent analysis uses an unfiltered light curve, as described later in this section.

A tunable parameter in the PM method is the segment size over which the time delay (TD) is measured. Shorter segments offer finer

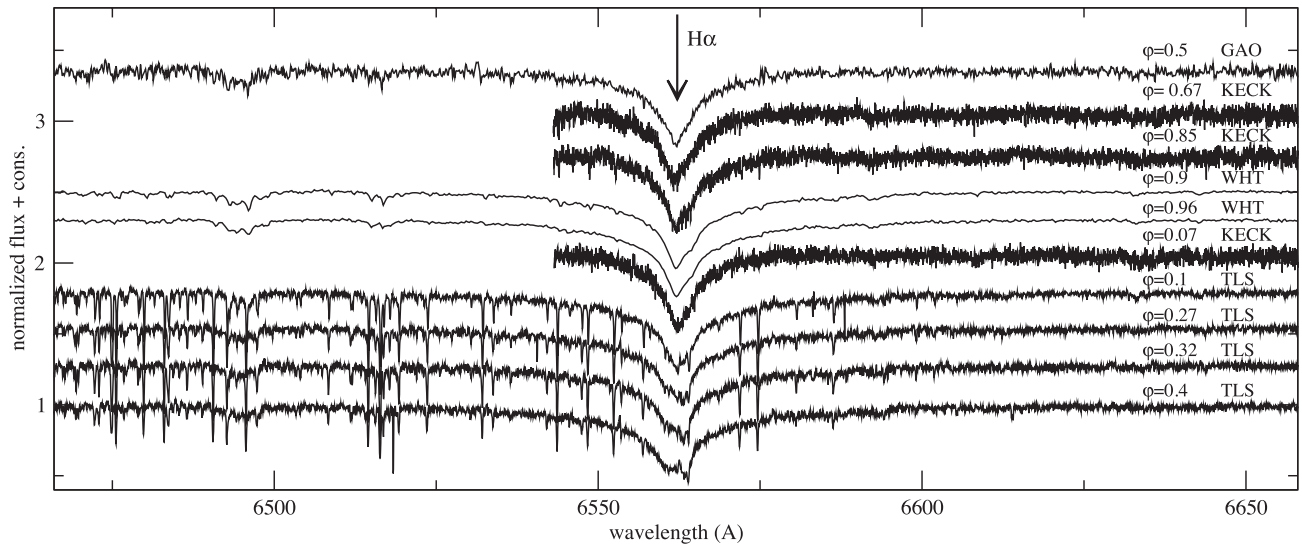

Figure 2. Selected spectra at different orbital phases, showing the effect of binary motion in the Hα line. The phases (as inferred in Section 3) and the observatories are given above each spectrum.

Table 2. RV measurements. HJD is shown without the prepending '24'.

HJD	RV_1 ($km\,s^{-1}$)	RV_2 ($km\,s^{-1}$)	Observatory
56048.53828	− 20.4 ± 0.9	− 12.8 ± 1.6	GAO
56086.73189	− 44.6 ± 1.8	− 16.1 ± 3.0	WHT
56089.55007	− 39.1 ± 1.7	− 9.0 ± 2.8	WHT
56092.55340	− 38.6 ± 1.8	− 16.5 ± 2.8	WHT
56228.66885	44.6 ± 0.6	–	APO
56557.73272	− 40.4 ± 0.8	–	APOGEE
56559.72264	− 37.8 ± 0.6	–	APOGEE
56560.72038	− 38.5 ± 0.5	–	APOGEE
56584.63151	− 22.3 ± 0.6	–	APOGEE
56585.63001	− 20.8 ± 0.5	–	APOGEE
57569.08281	− 24.2 ± 0.5	− 19.9 ± 0.5	KECK
57583.93289	− 44.2 ± 0.5	− 15.4 ± 0.5	KECK
57601.08965	− 41.7 ± 0.5	− 10.3 ± 0.5	KECK
57621.94122	− 29.8 ± 0.5	− 18.7 ± 0.5	KECK
57622.34135	− 31.8 ± 0.5	− 12.4 ± 1.0	TLS
57624.42425	− 30.3 ± 0.6	− 15.2 ± 1.0	TLS
57624.45236	− 30.6 ± 0.5	− 15.2 ± 0.9	TLS
57641.38582	4.7 ± 0.5	− 38.6 ± 1.0	TLS
57642.37919	8.4 ± 0.5	− 41.4 ± 1.0	TLS
57643.47454	12.5 ± 0.5	− 45.1 ± 1.4	TLS
57644.48464	15.7 ± 0.6	− 48.6 ± 1.5	TLS
57645.49054	15.7 ± 0.5	− 51.9 ± 1.3	TLS
57653.34960	44.9 ± 0.4	− 63.8 ± 1.3	TLS
57718.72473	− 28.9 ± 0.6	− 18.6 ± 0.6	KECK
58214.98802	17.6 ± 0.6	− 54.5 ± 1.1	APO

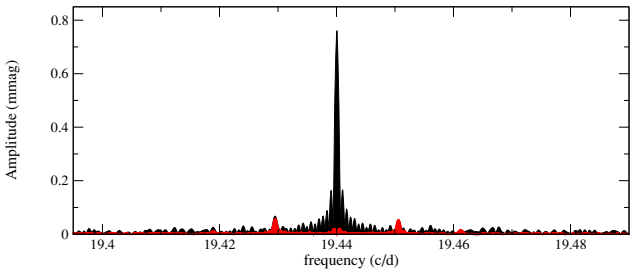

Figure 3. Fourier transform of the light curve at the strongest oscillation frequency (black). Strong sidelobes exist as a result of binary motion, separated from the main peak by the orbital frequency. At twice the orbital frequency from the main peak, smaller sidelobes are evident, indicating an eccentric orbit (Shibahashi, Kurtz & Murphy 2015). The orbital sidelobes remain even after prewhitening the pulsation peak (red).

sensitivity to the orbit at periastron, but lead to larger uncertainties per measurement and poorer frequency resolution in the Fourier transform (Murphy et al. 2014). We experimented with segment sizes of 2, 4, 6, 8, and 10 d and found 4 d to be optimal for this target. We used the nine strongest Fourier peaks in the high-pass filtered light curve for the PM analysis, carefully avoiding Nyquist aliases (Murphy, Shibahashi & Kurtz 2013), resulting in the TDs shown in Fig. 5. We ran the Markov Chain Monte Carlo (MCMC) code of Murphy et al. (2016b) on the weighted average TD to obtain the orbital parameters given in Table 3. The orbital solution is shown in Fig. 6.

3.2 Spectroscopic orbit determination

RVs were determined by cross-correlating the spectra with a well-matching synthetic template spectrum from the extensive spectral

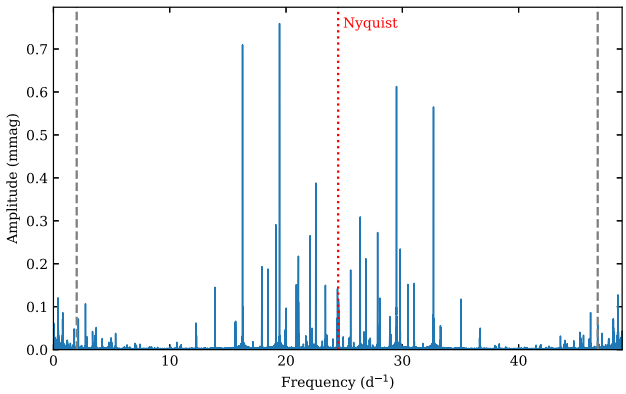

Figure 4. The Fourier spectrum of KIC 5709664 based on the 4-yr LC *Kepler* data set. The dotted red line is the Nyquist frequency. Some real peaks lie above the Nyquist frequency, and can be distinguished from their aliases by amplitude. The dashed grey lines delimit the frequency region considered for frequency extraction (see Section 4).

library of Munari et al. (2005). The calculated cross-correlation functions (CCFs) were fitted with two-component Gaussian functions, whose centroids gave the RVs for each component. Deviation from the Gaussian shape typically occurred around 100–150 $km\,s^{-1}$ away from the maxima.

After extracting the RVs, we computed the RV curve. For this we used our own MCMC-based RV fitting code, implementing the Metropolis–Hastings algorithm. The RVs and the fit for each component are plotted in Fig. 7 and the corresponding parameters are listed in Table 3.

3.3 A combined approach

The RV and PM methods are complementary. When used together, they offer a much longer observational span that allows the orbital parameters to be refined. They also allow the TDs to be allocated to one of the two components of the RV curve. While RVs constitute a near-instantaneous measurement of the orbit, our TD data used a 4-d integration and therefore undersample the orbit at periastron. We used the correction described by Murphy et al. (2016b) to account for this.

We found that the RV_2 velocities belong to the pulsating star for which the TDs were measured. To refine the orbit, we ran the PM MCMC algorithm on the joint data set without applying any additional weights, resulting in the parameters in the final column of Table 3.

4 FREQUENCY ANALYSIS

4.1 Extraction of p modes

We used the orbit determined in Section 3.3 to correct the light arrival times to the barycentre of the binary system, so that there was no longer any FM of any of the pulsation modes. This leads to the cleanest Fourier spectrum, with no orbital sidelobes on any pulsation peaks, for analysis of the pulsation content.

We used the PERIOD04 software (Lenz & Breger 2004) to identify pulsation frequencies in these data and to fit them to the light curve in order to compute their amplitudes and phases. We used the 'super-Nyquist asteroseismology' method (Murphy et al. 2013) to distinguish the Nyquist aliases from the real oscillation frequencies without recourse to the *Kepler* SC data. Below 2 d^{-1} there are

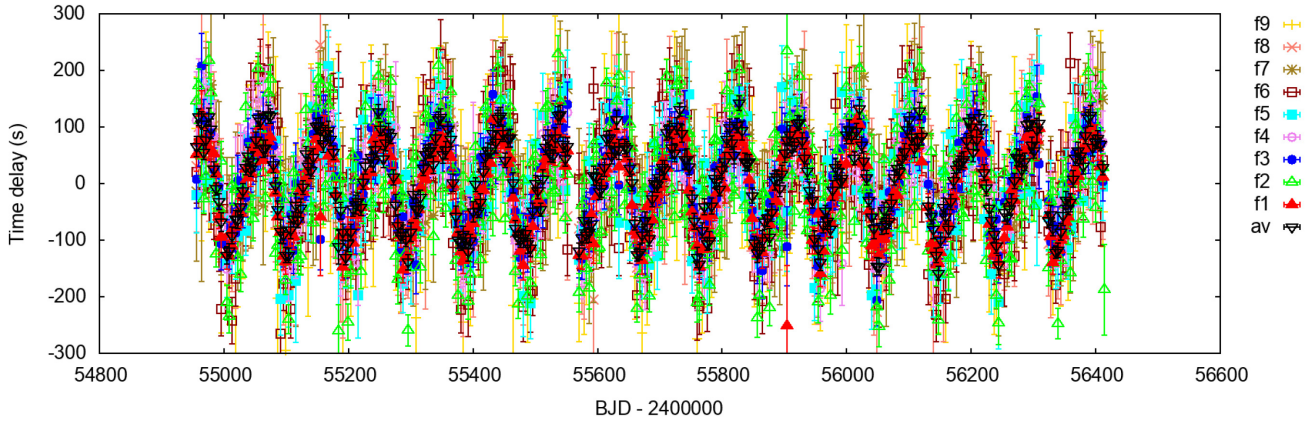

Figure 5. TDs for the nine strongest modes of KIC 5709664 and the weighted average TD (black), at 4-d sampling in the full 4-yr light curve.

Table 3. Orbital parameters for the KIC 5709664 system. Only one component pulsates, so the TD orbit cannot extract parameters for the second star. The RV and TD+RV orbits used velocities from both components. The semimajor axes are given in light seconds, where 1 light second = 299 792 458 m ≈ 0.431 $R_\odot$ ≈ 0.002 au.

Parameter	Units	TD only	RV only	TD + RV
P_{orb}	d	$95.024^{+0.031}_{-0.034}$	$94.9735^{+0.023}_{-0.023}$	$94.9854^{+0.0058}_{-0.0057}$
e		$0.51^{+0.020}_{-0.021}$	$0.57^{+0.015}_{-0.015}$	$0.547^{+0.0036}_{-0.0037}$
ϖ	rad	$0.398^{+0.037}_{-0.028}$	$0.354^{+0.034}_{-0.034}$	$0.388^{+0.013}_{-0.0096}$
t_p	d	$2\,454\,993.33^{+0.57}_{-0.49}$	$2\,454\,993.42^{+0.66}_{-0.66}$	$2\,454\,993.8^{+0.21}_{-0.19}$
$f(m_1, m_2, \sin i)$	$M_\odot$	$0.1872^{+0.0096}_{-0.0090}$	$0.1566^{+0.009}_{-0.009}$	$0.1666^{+0.0045}_{-0.0046}$
$f(m_2, m_1, \sin i)$	$M_\odot$	–	$0.5438^{+0.028}_{-0.028}$	$0.5638^{+0.0153}_{-0.0155}$
$a_1 \sin i/c$	s	$116.3^{+2.0}_{-1.9}$	$109.5^{+3.3}_{-3.3}$	$111.9^{+1.0}_{-1.0}$
$a_2 \sin i/c$	s	–	165.8^{+3}_{-3}	$166.8^{+0.65}_{-0.64}$
q		–	$0.6602^{+0.065}_{-0.065}$	$0.6706^{+0.0065}_{-0.0068}$
K_1	km s^{-1}	$31.05^{+0.94}_{-0.88}$	$30.62^{+1.02}_{-1.02}$	$30.67^{+0.31}_{-0.31}$
K_2	km s^{-1}	–	$46.37^{+1.08}_{-1.08}$	$45.74^{+0.20}_{-0.20}$
v_γ	km s^{-1}	–	$-22.01^{+0.3}_{-0.3}$	-21.94

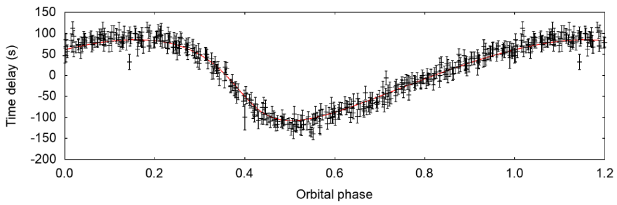

Figure 6. The weighted average TDs folded on the orbital solution, shown with the best-fitting orbit computed using these TDs, only. The phase is calculated with respect to the time stamp of the first TD measurement, BJD = 2454955.53140. The χ^2/N of the fit was 0.75.

some incoherent peaks in the Fourier transform, presumably from spots and rotation on one of the stars (discussed below), so we did not extract pulsation frequencies below 2 d^{-1}. Frequencies were extracted in this manner down to 20 μmag, resulting in the 38 frequencies, amplitudes, and phases shown in Table 4. While further significant peaks could be extracted below the 20 μmag threshold, these are of decreasing significance and it is not possible to model so many frequencies in δ Sct stars at present, so we ceased frequency extraction here. Our lowest amplitude frequency has a 10σ significance. The Fourier residuals after our frequency extraction are shown in Fig. 8.

We note that the strongest two frequencies, at 19.4401 and 16.2596 d^{-1}, have a period ratio of 0.836, consistent with the expected ratio for the third and second radial overtone modes (Smolec et al. 2017).

4.2 Low frequencies

At low frequencies there are broad power excesses (Fig. 9), which were not extracted with the p modes. They might be attributed to spots on a rotating star. Since the primary is a δ Sct star with a mass likely in the region 1.5–2.0 $M_\odot$, the measured mass ratio of 0.67 (Table 3) gives a companion mass in the range 1.0–1.34 $M_\odot$, which should have a surface convection zone capable of generating sun-like star-spots. As these star-spots migrate over the surface and as the star rotates, these cause brightness variations. Such star-spot-induced variability has been detected in thousands of *Kepler* light curves (Nielsen et al. 2013; McQuillan, Mazeh & Aigrain 2014). We show a 15-d segment of the residual light curve that illustrates the typical rotational modulation from sun-like star-spots in Fig. 10.

Also evident in the low-frequency region of the Fourier transform (Fig. 9) at 1.78 d^{-1} is a signature of r modes, which appear to

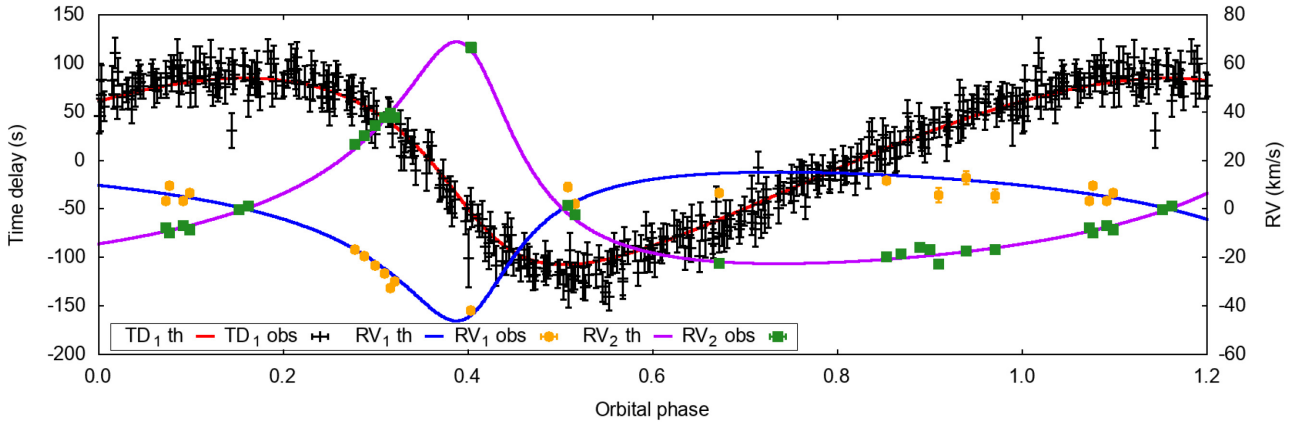

Figure 7. Combined RV and TD data set for KIC 5709664, with the best-fitting solution plotted as solid lines. The χ^2/N of this combined fit was 2.55.

Table 4. The 38 extracted frequencies in descending amplitude order. The time zero-point for the phases is BJD = 2455688.77. All amplitudes have the same uncertainty.

Frequency (d^{-1})	Amplitude (mmag ± 0.0024)	Phase ($-\pi$ to $+\pi$)
19.440 055 ± 0.000 001	0.765	2.093 ± 0.003
16.259 601 ± 0.000 001	0.712	− 0.846 ± 0.003
22.558 025 ± 0.000 002	0.388	2.446 ± 0.006
19.123 847 ± 0.000 003	0.294	− 0.785 ± 0.008
27.875 417 ± 0.000 003	0.274	− 2.343 ± 0.009
22.075 406 ± 0.000 003	0.265	0.075 ± 0.009
17.919 903 ± 0.000 005	0.194	− 1.515 ± 0.013
18.452 354 ± 0.000 005	0.187	− 0.211 ± 0.013
25.555 143 ± 0.000 005	0.186	0.918 ± 0.013
20.883 914 ± 0.000 006	0.151	− 0.299 ± 0.016
13.902 632 ± 0.000 006	0.144	− 1.392 ± 0.017
24.424 301 ± 0.000 007	0.141	− 1.782 ± 0.017
16.311 322 ± 0.000 008	0.111	2.630 ± 0.022
2.752 339 ± 0.000 009	0.107	0.511 ± 0.023
20.015 493 ± 0.000 009	0.100	− 2.862 ± 0.024
24.557 842 ± 0.000 010	0.091	2.590 ± 0.027
2.139 325 ± 0.000 013	0.072	− 1.483 ± 0.034
15.663 759 ± 0.000 014	0.067	− 0.801 ± 0.036
12.236 958 ± 0.000 015	0.062	− 2.568 ± 0.039
15.636 912 ± 0.000 015	0.061	− 2.276 ± 0.040
3.679 324 ± 0.000 018	0.051	2.898 ± 0.047
22.237 565 ± 0.000 018	0.051	1.360 ± 0.047
22.252 450 ± 0.000 019	0.048	0.653 ± 0.050
19.907 823 ± 0.000 019	0.047	− 2.338 ± 0.051
3.361 601 ± 0.000 021	0.043	− 2.718 ± 0.057
5.345 200 ± 0.000 024	0.038	− 1.275 ± 0.063
24.374 664 ± 0.000 024	0.038	1.902 ± 0.064
23.471 627 ± 0.000 026	0.036	− 2.328 ± 0.068
12.296 338 ± 0.000 027	0.034	− 1.905 ± 0.071
23.529 187 ± 0.000 029	0.032	2.360 ± 0.076
3.563 488 ± 0.000 029	0.032	1.171 ± 0.077
21.697 655 ± 0.000 029	0.031	− 2.938 ± 0.078
2.865 545 ± 0.000 031	0.030	0.025 ± 0.082
24.917 230 ± 0.000 032	0.029	1.558 ± 0.084
4.955 035 ± 0.000 033	0.028	− 1.029 ± 0.088
4.195 776 ± 0.000 036	0.025	− 2.610 ± 0.096
27.160 243 ± 0.000 038	0.024	− 0.892 ± 0.100
27.867 651 ± 0.000 038	0.024	3.101 ± 0.100

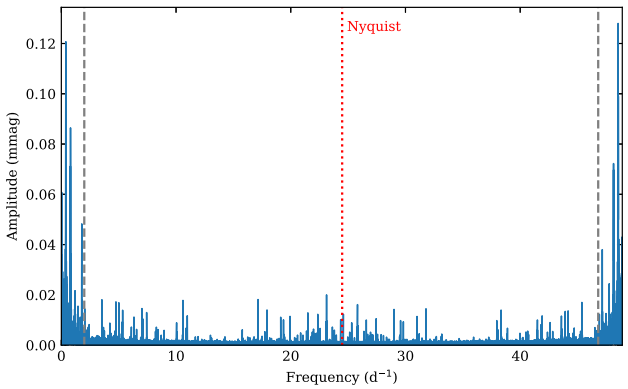

Figure 8. The Fourier residuals after the 38-frequency fit. The dotted red line is the Nyquist frequency and the dashed grey lines delimit the frequency region considered for frequency extraction. The low-frequency region is shown in Fig. 9.

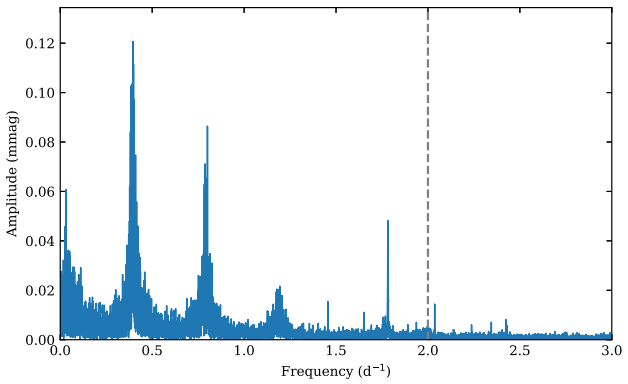

Figure 9. The Fourier transform of the low-frequency region, after the 38-frequency fit. The dashed grey line delimits the frequency region above which peaks were extracted. The three broad humps might be from spots and rotation on the secondary component. The feature at 1.78 d^{-1} could be attributed to r modes.

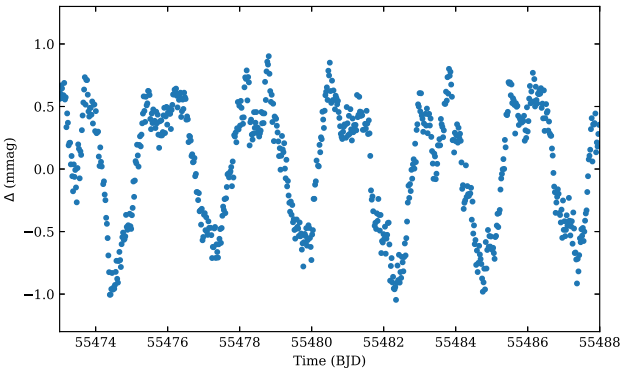

Figure 10. A 15-d segment of the residual light curve (with the 38-frequency fit subtracted), showing the low-frequency variability that we attribute to star-spots on the cooler companion.

be ubiquitous among A stars (Saio et al. 2018). The morphology is a 'hump and spike', of which the spike is believed to be the rotation frequency of the star, mechanically generating r modes that are visible as the hump. If the r modes are attributable to the primary, the spike suggests a rotation frequency of 1.782 d^{-1} and a corresponding period of 0.561 d for this component, consistent with typical rotation periods of A-type stars (Royer, Zorec & Gómez 2007). Similarly, if we take the first Fourier hump of the secondary's star-spot signature as the rotation frequency, noting that there are potential caveats to this interpretation (McQuillan et al. 2014; Angus et al. 2018), then we obtain a rotation frequency for the secondary of 0.395 d^{-1}, corresponding to a period of 2.53 d. While this is relatively rapid for a star of this mass, the shorter pre-main-sequence phase of the more massive primary will have limited early rotational braking via disc locking, and left the secondary rotating relatively rapidly.

5 CONCLUSIONS AND SUMMARY

We analysed *Kepler* long-cadence data of the hybrid δ Sct/γ Dor star KIC 5709664. The frequency analysis of the photometric data revealed Fourier peaks with sidelobes, suggesting binary orbital motion. We used the nine strongest Fourier peaks for the PM analysis and determined the orbital parameters.

We obtained 25 medium- and high-resolution spectra at six observatories, which unambiguously confirmed the binary nature. The calculated CCFs were fitted with a two-component Gaussian function and the RV curves of each binary component were fitted to measure the orbital parameters.

Although the parameters determined by the two independent methods are in good agreement, we performed a combined RV and PM approach to determine more accurate orbital parameters that are listed in the final column of Table 3. We found that the pulsating star for which the TDs are measured is the component to which the RV_2 velocities belong.

We performed frequency analysis of the data, and extracted 38 frequencies with amplitudes greater than 20 μmag. At low frequencies, we found broad power excesses which are likely attributed to spots on the rotating surface of the primary component. Since the primary is a δ Sct star with a mass likely in the region 1.5–2.0 $M_\odot$, the measured mass ratio of 0.67 gives a companion mass in the range 1.0–1.34 $M_\odot$, which should have a surface convection zone capable of generating sun-like star-spots. We also found a signature of r modes, presumably belonging to the primary. We inferred rotation periods of 0.56 and 2.53 d for the primary and secondary, respectively.

ACKNOWLEDGEMENTS

This project has been supported by the Hungarian NKFI Grants K-113117, K-115709, K-119517, and KH-130372 of the Hungarian National Research, Development and Innovation Office. AD was supported by the ÚNKP-18-4 New National Excellence Program of the Ministry of Human Capacities and the János Bolyai Research Scholarship of the Hungarian Academy of Sciences. AD would like to thank the City of Szombathely for support under Agreement No. 67.177-21/2016. SJM is a DECRA fellow supported by the Australian Research Council (grant number DE180101104). This project has been supported by the Lendület Program of the Hungarian Academy of Sciences, project No. LP2018-7/2018. SzM has been supported by the Premium Postdoctoral Research Program of the Hungarian Academy of Sciences. HL was supported by the DFG grant LE 1102/3-1.

Based on observations obtained with the APO 3.5-m telescope, which is owned and operated by the Astrophysical Research Consortium. IRAF is distributed by the National Optical Astronomy Observatories, which are operated by the Association of Universities for Research in Astronomy, Inc., under cooperative agreement with the National Science Foundation.

REFERENCES

Abolfathi B. et al., 2018, ApJS, 235, 42
Alfonso-Garzón J., Montesinos B., Moya A., Mas-Hesse J. M., Martín-Ruiz S., 2014, MNRAS, 443, 3022
Angus R., Morton T., Aigrain S., Foreman-Mackey D., Rajpaul V., 2018, MNRAS, 474, 2094
Blanton M. R. et al., 2017, AJ, 154, 28
Borucki W. J. et al., 2010, Science, 327, 977
Eisenstein D. J. et al., 2011, AJ, 142, 72
García Pérez et al., 2016, AJ, 151, 144
Gilliland R. L. et al., 2010, PASP, 122, 131
Jenkins J. M. et al., 2010a, ApJ, 713, L87
Jenkins J. M. et al., 2010b, ApJ, 713, L120
Koch D. G. et al., 2010, ApJ, 713, L79
Lampens P. et al., 2018, A&A, 610, A17
Lenz P., Breger M., 2004, Commun. Asteroseismol., 144, 41
Majewski S. R. et al., 2017, AJ, 154, 94
McQuillan A., Mazeh T., Aigrain S., 2014, ApJS, 211, 24
Munari U., Sordo R., Castelli F., Zwitter T., 2005, A&A, 442, 1127
Murphy S. J., Shibahashi H., 2015, MNRAS, 450, 4475
Murphy S. J., Shibahashi H., Kurtz D. W., 2013, MNRAS, 430, 2986
Murphy S. J., Bedding T. R., Shibahashi H., Kurtz D. W., Kjeldsen H., 2014, MNRAS, 441, 2515
Murphy S. J., Bedding T. R., Shibahashi H., 2016a, ApJ, 827, L17
Murphy S. J., Shibahashi H., Bedding T. R., 2016b, MNRAS, 461, 4215
Murphy S. J., Moe M., Kurtz D. W., Bedding T. R., Shibahashi H., Boffin H. M. J., 2018, MNRAS, 474, 4322
Nielsen M. B., Gizon L., Schunker H., Karoff C., 2013, A&A, 557, L10
Royer F., Zorec J., Gómez A. E., 2007, A&A, 463, 671
Saio H., Kurtz D. W., Murphy S. J., Antoci V. L., Lee U., 2018, MNRAS, 474, 2774
Sánchez Arias J. P., Córsico A. H., Althaus L. G., 2017, A&A, 597, 29
Shibahashi H., Kurtz D. W., 2012, MNRAS, 422, 738
Shibahashi H., Kurtz D. W., Murphy S. J., 2015, MNRAS, 450, 3999
Shporer A. et al., 2016, ApJ, 829, 34

Smolec R., Dziembowski W., Moskalik P., Netzel H., Prudil Z., Skarka M., Soszynski I., 2017, EPJ Web Conf., 152, 06003
Stumpe M. C., Smith J. C., Catanzarite J. H., Van Cleve J. E., Jenkins J. M., Twicken J. D., Girouard F. R., 2014, PASP, 126, 100
Uytterhoeven K. et al., 2011, A&A, 534, A125
Wilson J. C. et al., 2012, in McLean I. S., Ramsay S. K., Takami H., eds, Proc. SPIE Conf. Ser. Vol. 8446, Ground-based and Airborne Instrumentation for Astronomy IV. SPIE, Bellingham, p. 84460H

[1]*ELTE Eötvös Loránd University, Gothard Astrophysical Observatory, 9700 Szombathely, Szent Imre herceg u. 112., Hungary*
[2]*Konkoly Observatory, Research Centre for Astronomy and Earth Sciences, Hungarian Academy of Sciences, H-1121 Budapest, Konkoly Thege Miklós út 15-17, Hungary*
[3]*MTA-ELTE Exoplanet Research Group, H-9700 Szombathely, Szent Imre h. u. 112, Hungary*
[4]*Sydney Institute for Astronomy, School of Physics, The University of Sydney, NSW 2006, Australia*
[5]*Stellar Astrophysics Centre, Department of Physics and Astronomy, Aarhus University, Ny Munkegade 120, DK-8000 Aarhus C, Denmark*
[6]*Institute of Physics, Eötvös University, H-1117 Budapest, Hungary*
[7]*MTA CSFK Lendület Near-Field Cosmology Research Group, 1121 Budapest, Konkoly Thege Miklós út 15-17, Hungary*
[8]*Baja Astronomical Observatory of Szeged University, H-6500 Baja, Szegedi út, Kt. 766, Hungary*
[9]*Department of Experimental Physics, University of Szeged, H-6720 Szeged, Dóm tér 9, Hungary*
[10]*Thüringer Landessternwarte Tautenburg, Karl-Schwarzschild-Observatorium, D-07778 Tautenburg, Germany*
[11]*Apache Point Observatory, Sunspot, NM 88349, USA*
[12]*Astrophysics Group, Keele University Newcastle-under-Lyme, Keele ST5 5BG, UK*
[13]*Department of Astrophysics/IMAPP, Radboud University Nijmegen, P.O. Box 9010, NL-6500 GL Nijmegen, the Netherlands*
[14]*Department of Astronomy, University of California at Berkeley, Berkeley, CA 94720-3411, USA*
[15]*Kavli Institute for Astrophysics and Space Research, M.I.T., Cambridge, MA 02139, USA*
[16]*California Institute of Technology, 1200 E. California Boulevard, Pasadena, CA 91125, USA*

This paper has been typeset from a TEX/LATEX file prepared by the author.